

**Title: Direct observation of magnetic vortex behavior in an ordered
 $\text{La}_{0.7}\text{Sr}_{0.3}\text{MnO}_3$ dot arrays**

Authors: Zhenghua Li¹, Dapeng Dong¹, Dedi Liu¹, Jia Liu¹, Dongping Liu^{1*}, and Xiang Li²

Author affiliations: ¹Liaoning Key Lab of Optoelectronic Films & Materials, School of Physics and Materials Engineering, Dalian Nationalities University, Dalian, 116600, China; ²School of Materials Science and Engineering, University of Shanghai for Science and Technology, Shanghai, 200093, China

Corresponding person: Dongping Liu (phone: +86-411-87508902, fax: +86-411-87508902, email: dongping.liu@dlnu.edu.cn)

SECTION 1: The importance of the triangular shaped geometry

In this paper we studied triangular dots that are of additional interest since the sharp corners of the polygonal nanoelements (triangles, square, etc) produce strong magnetostatic fields. The use of this quite simple triangular geometry provides an additional advantage of breaking the circular symmetry so making the vortex core, domain wall, as well as the chirality of the vortex well distinguishable by MFM technique. The understanding and control of the vortex states makes the triangular dots unique candidates for the applications for non-volatile magnetic storage such as vortex MRAM memories [16-17].

SECTION 2: More detailed description of sample preparation and experimental setup

The epitaxial LSMO thin films, approximately 40 nm thick, were deposited on (001) oriented SrTiO₃ (STO) substrates by pulsed laser deposition with a substrate temperature of 700°C. The KrF laser was operated at 248 nm and a fluence of about 1.0 J/cm². A double layer mask of 20 nm polymethyl methacrylate (PMMA) and 300 nm of hydrogen silsesquioxane (HSQ) was spin coated on LSMO and patterned using electron beam lithography. The mask pattern determines the areas that can be exposed to an Ar⁺ ion implantation at 80 keV and a dose of 1×10^{14} cm⁻². Finally, the PMMA can be used as a lift-off layer to remove the HSQ mask.

SECTION 3: The demonstration of the in-field magnetic force microscopy technique

Magnetic force microscopy is well suited to exploring ferromagnetic domain structures. However, the resolution of the MFM system cannot be improved simply by reducing the tip-to-sample distance, at that point MFM mixes magnetic, Van der Waals, and electrostatic forces. Therefore, the actual resolution of MFM is at least an order of magnitude lower than the resolution of atomic force microscopy (AFM). Here, we demonstrated an in-field magnetic force microscopy (IF-MFM) to locally observe the magnetic vortex in triangular arrays with very high spatial resolution. This technique uses an *ex situ* MFM tip reversal method to achieve an optimized separation of the topography and magnetic signal. Firstly, the MFM tip was *ex situ*

magnetized along the tip axis, tapping and lift mode AFM/MFM scans were carried out using a high-coercivity MFM tip with a coating of a 20 nm L1₀-FePt film (The MFM tip with high coercivity is effective to suppress the oscillation of its magnetization, and consequently to obtain microscopic magnetic domains with high resolution). Secondly, the MFM tip was *ex situ* reversed by applying an external magnetic field, the corresponding MFM images can be detected with opposite MFM contrast. Thirdly, by subtraction of the two MFM signals with inverted tip magnetizations, the topographic information can be removed. Based on the *ex situ* MFM tip reversal technique, we can perform a near surface MFM imaging by precisely reducing the tip-sample distance without mixing the atomic force. Thus, the spatial resolution can be greatly improved. In addition, by using the deconvolution technique and micromagnetics, we are able to quantify the measured MFM images, and precisely analyze the magnetic domain variations, as well as the domain wall motions in nanometer length scales.

Figure S1 shows the principle of the *ex situ* MFM tip reversal technique with (a) MFM tip magnetized upwards and (b) MFM tip magnetized downwards. The MFM images containing both the magnetic and topographic contributions, these two contributions can be completely separated by summation and subtraction of the two MFM images with inverted tip magnetizations. Figure S2 shows (a) topographic image, (b) In-field MFM phase image, and (c) conventional MFM phase image of a perpendicular recording medium. The experiment was conducted very near the sample surface with a lift height of -30 nm. The oscillation frequency (f_0) is approximately 256 kHz. Tapping and lift mode AFM/MFM scans were carried out using a high-coercivity FePt tip. It is found that the magnetic domains of the recorded bits can be clearly observed in the In-field MFM image, while the magnetic signals cannot be resolved in the case of conventional MFM with the same experimental conditions. Therefore, the resolution of the MFM image can be greatly improved by In-field MFM technique.

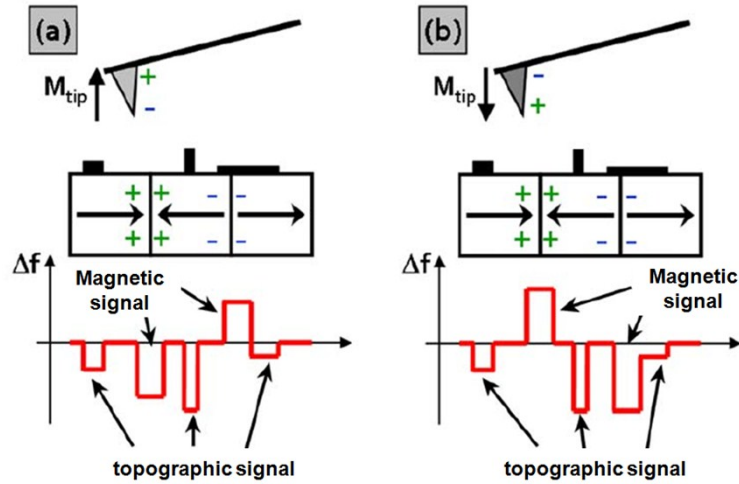


Figure S1 the principle of the *ex situ* MFM tip reversal technique with (a) MFM tip magnetized upwards and (b) MFM tip magnetized downwards

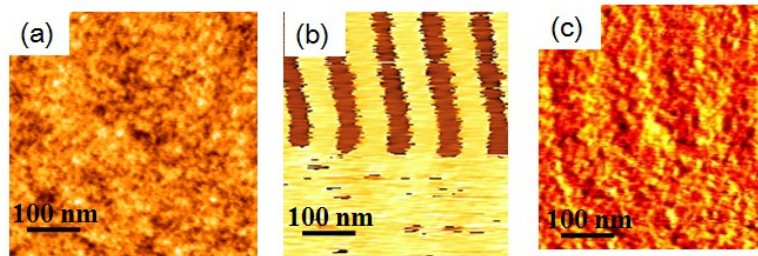


Figure S2 (a) topographic image, (b) In-field MFM phase image, and (c) conventional MFM phase image of a perpendicular recording medium

The present technique can be applied to investigate the microscopic magnetic domain structures in a variety of magnetic materials, such as high-density recording media, ultrathin films, nanoparticles, patterned elements, as well as other magnetic features and nanostructures, which allows a wide range of future applications, for example, in data storage and biomedicine.

SECTION 4: The systematic control of the CW/ACW chirality in square dots using the magnetostatic-coupled nanomagnet

Here, we show that the chirality of the vortex can be deterministically controlled in the LSMO square dots by using a magnetostatic-coupled nanomagnet, as indicated in Figures S3 (a) to (d). The arrays in Figures S3 (a) and (b) were magnetized by an external field of 79.58 KA/m in advance. At remanence, the island relaxes to a stable CW or ACW structure with the core appeared near the center. It also found that the direction of the magnetic moments of the island is antiparallel to the magnetization direction of the adjacent nanomagnet. The similar behavior can also be found in the

square dot with the external field reversed from -79.58 kA/m to 0 , as seen in Figures S3 (c) and (d). Therefore, the controlling of the CW/ACW chirality in confined geometries can be achieved in the presence of magnetostatic-coupled nanomagnet with specially designed geometries.

Figures S3 (e) to (j) present the micromagnetic simulation results of selective chirality control in a single island using the magnetostatic-coupled nanomagnet. The dimensions of a single dot as well as the coupled nanomagnet have been set to be consistent with experimental results. In simulation, the domain evolution process of the vortex structure has been presented by applying an external field varying from -79.58 kA/m to 0 kA/m . When the applied field reaches the maximum field of -79.58 kA/m (Figure S3 (e)), all the magnetic moments of the structure are coherently reversed along the applied field direction. As the driven field gradually reduces, the bias nanomagnets favor to form a well-defined magnetic structure dominated by the geometrically induced shape anisotropy, whereas in-homogeneous magnetization distribution in the center island can be observed, as shown in Figure S3 (f). It is seen that the magnetization configuration of the island exhibits a concave down character due to magnetostatic interactions with the nearest nanomagnet. This mechanism causes a selective chirality control in the islands relating to the magnetic configurations of the adjacent nanomagnet with specially designed geometries. Finally, vortex retains a stable CW or ACW structure in the remanent state with the core appeared near the center of the island (Figure S3 (g) or Figure S3 (j)). Figures S3 (h) to (j) present the opposite features of the vortex structure with the driven field reversed from -79.58 kA/m to 0 , as compared with Figures S3 (e) to (g).

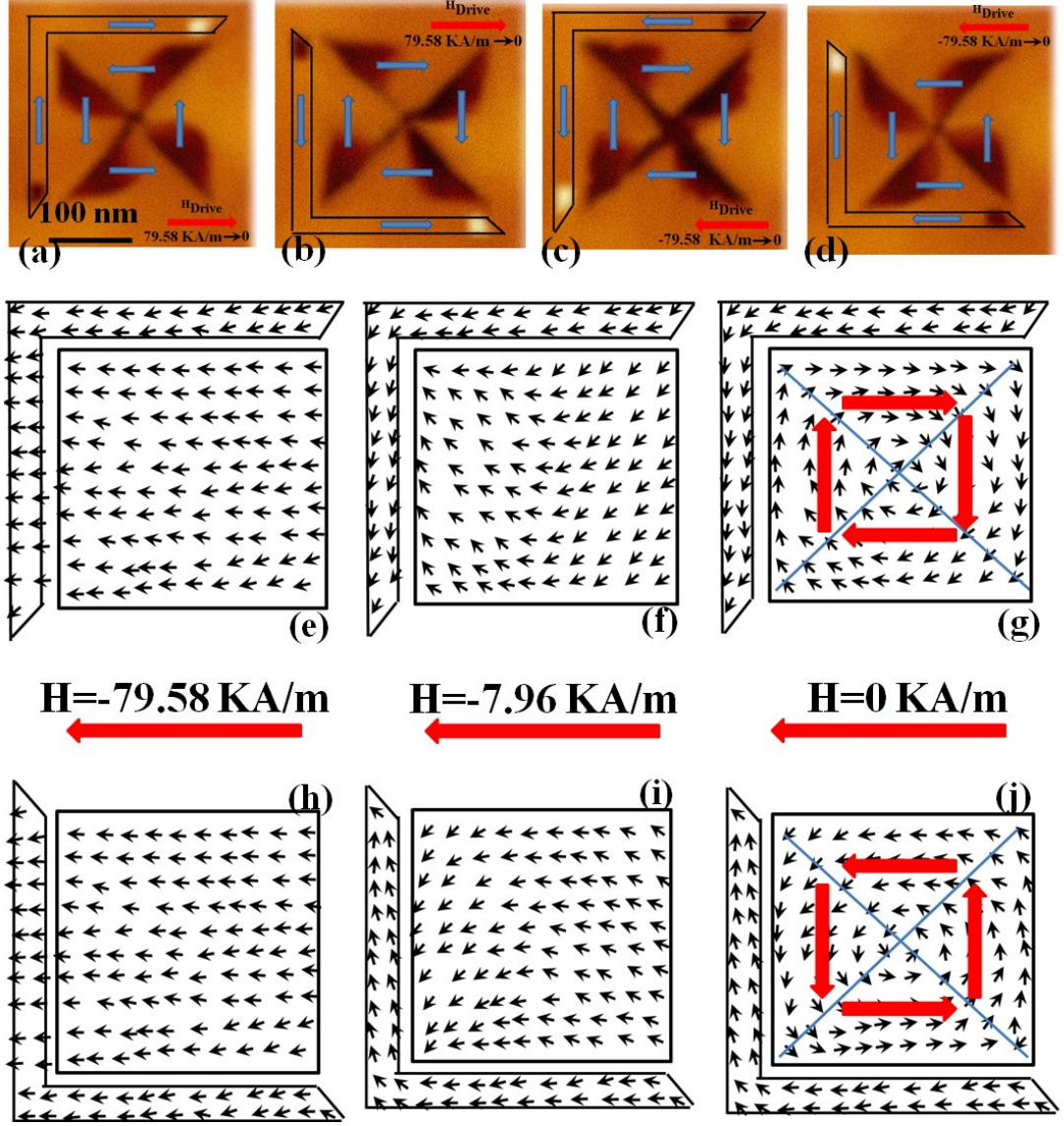


Figure S3 The systematic control of the CW/ACW chirality in square dots using the magnetostatic-coupled nanomagnet

SECTION 5: The physical description of the micromagnetic model

In the micromagnetic modeling, the total energies in the i th grid includes the Zeeman energy, crystalline anisotropy energy, magnetoelastic energy, shape anisotropy energy, exchange interaction, and magnetostatic interaction,

$$E^i_{total} = E^i_{Zee} + E^i_{ck} + E^i_{m-el} + E^i_{sk} + E^i_{ex} + E^i_m \quad (1)$$

The effective field H^i_{eff} acting on each magnetic moment can be defined as the derivative of energy with respect to local magnetization \hat{M}^i ,

$$\mathbf{H}_{eff}^i = -\frac{1}{\mu_0} \frac{\partial E^i}{\partial \mathbf{M}^i} \quad (2)$$

Differentiating of Eq. (1) gives an effective field H_{eff}^i which consists of several components:

$$\mathbf{H}_{eff}^i = \mathbf{H}_{Zee}^i + \mathbf{H}_{ck}^i + \mathbf{H}_{m-el}^i + \mathbf{H}_{sk}^i + \mathbf{H}_{ex}^i + \mathbf{H}_m^i \quad (3)$$

From Eq. (3), the effective field in each grid is contributed by five terms: the external field, the crystalline anisotropy field, the magnetoelastic field, the shape anisotropy field, the exchange interacting field and the demagnetising field.

At equilibrium state, the magnetization vector \mathbf{M}^i prefers to rotate parallel to the effective field \mathbf{H}_{eff}^i for energy minimization, the magnetization reversal process is accomplished based on the Landau-Lifshitz-Gilbert (LLG) equation.

$$\frac{d\mathbf{M}^i}{dt} = -\gamma \mathbf{M}^i \times \mathbf{H}_{eff}^i - \frac{\alpha}{M_s} \mathbf{M}^i \times (\mathbf{M}^i \times \mathbf{H}_{eff}^i) \quad (4)$$

where M_s is the saturation magnetization, γ is the gyromagnetic constant, and α is the damping coefficient.

SECTION 6: The dominant role of shape and magnetocrystalline anisotropy energies on the domain structure

Here, we performed the micromagnetic simulations (the micromagnetic program has been developed by our research group using FORTRAN language) to explain the magnetic domain structures in the patterned LSMO dot arrays. The following parameters were used: a saturation magnetization of 460 emu/cm³ (at room temperature), biaxial magnetocrystalline anisotropy constant of 1.5×10⁴ ergs/cm³. It is deduced that the shape anisotropy combined with the biaxial magnetocrystalline anisotropy energy of the islands dominates over other magnetic effects to determine the magnetic domain structures, as indicated in Figure S4. For the (001)-oriented LSMO rectangular islands, the domain evolves from single flux-closed domain states to multiple flux-closed domain states as the aspect ratio (the ratio of height/width) gradually increases, however, when the shape of the island changed to an elongated

hexagonal dot, the domain structure changes from multiple flux-closed domain state to a single domain, as shown in Figure S4 (a). Here the domain structure is a competition between the biaxial magnetocrystalline anisotropy and the geometrically induced shape anisotropy. In the case of the uniaxial-oriented LSMO rectangular islands, it appears the vortex domains for aspect ratios smaller than 2 and a single domain state for larger aspect ratios above 2, indicating a delicate balance between the uniaxial anisotropy and shape anisotropy, as indicated in Figure S4 (b).

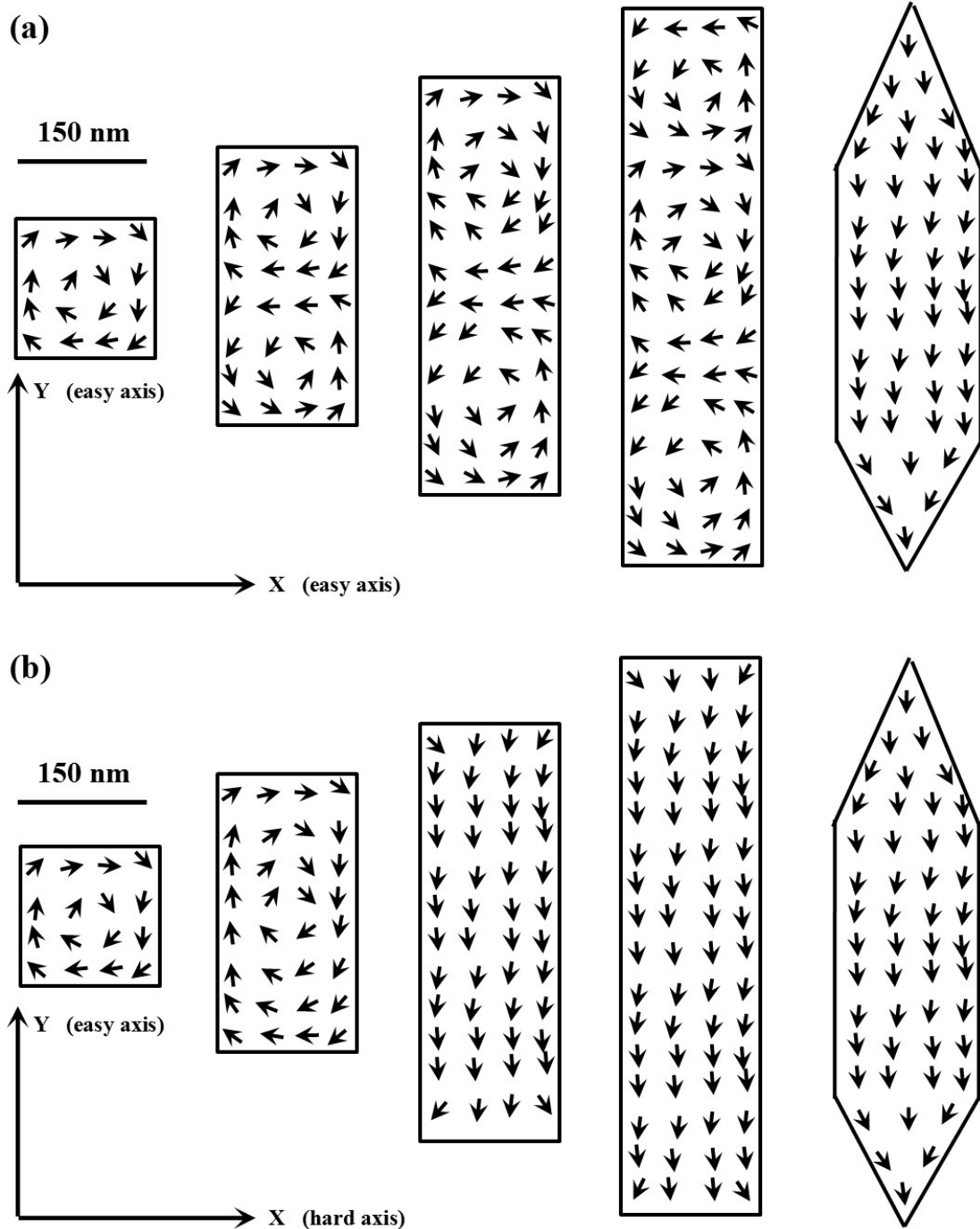


Figure S4 The dominant role of shape and magnetocrystalline anisotropy energies on the domain structure